Decoupled Power Control for A Modular Multilevel Converter-Based Hybrid AC-DC Grid Integrated with Hybrid Energy Storage

Lei Zhang, *Student Member*, *IEEE,* Yi Tang, *Senior Member*, *IEEE*, Shunfeng Yang, *Student Member, IEEE,* and Feng Gao, *Member*, *IEEE*

***Abstract*—This paper presents a decoupled power control strategy for a modular multilevel converter (MMC)-based hybrid ac-dc grid integrated with a hybrid energy storage system (HESS). This system can mitigate the active power fluctuations caused by intermittent renewable generation and also realize reactive power compensation as required by voltage regulation. The proposed hybrid ac-dc system is novel in that batteries and supercapacitors are distributed into the upper arm and the lower arm of the MMC, respectively. It is therefore possible to design fully decoupled power control and simultaneously optimize the performances of batteries and supercapacitors. Firstly, the system modeling and operational principles of the MMC are briefly introduced in this paper. Based on these analyses, the power decoupling between the upper arm and the lower arm is presented to realize different control objectives. Moreover, battery state-of-charge (SOC) balancing control and supercapacitor voltage control are also presented, which are crucial for ensuring the normal operation of these energy storage components and the proposed MMC-based hybrid ac-dc grid. Finally, the proposed system and its control strategies are verified by laboratory experimental results.**

***Index Terms*—decoupled power control; hybrid energy storage system; modular multilevel converter.**

I. Introduction

Hybrid ac-dc grids have recently attracted a lot of research attentions as many distributed generation, energy storage, and energy-efficient electronic loads found in the modern distribution systems work with dc power. Several coordination and supervisory control strategies of hybrid ac-dc grids have been deeply investigated in [1]-[9]. Due to the increasing penetration of renewable energy sources (RES), energy storage systems (ESSs) are required to deal with the power fluctuations caused by such intermittent generation sources. Because of the high energy density and stability of long-term operation, batteries are commonly used in the ESSs integrated with wind farms and photovoltaic (PV) power plants. However, for areas with frequent weather changes, ESS is also required to compensate the short-term fluctuations with high power rating, which will induce rapid charging or discharging of batteries. As mentioned in [10], the continuous high-current operation may lead to battery degradation and severely shorten the lifetime of batteries.

To mitigate the battery degradation caused by frequent and high power fluctuations, supercapacitors (SCs) with high power density are commonly combined with batteries to form a hybrid energy storage system (HESS). As analyzed in [11-13], by diverting different forms of power fluctuations into batteries and SCs, HESS can make full use of the advantages of these two energy storage components, which can help reduce the size and capacity of the overall system, and extend the lifetime of batteries and attenuating the thermal stresses of batteries.

Conventional hybrid ac-dc microgrids and HESSs are mainly based on two-level converters and dc-dc converters, where batteries and SCs are integrated with the dc bus through paralleled dc-dc converters or multi-input dc-dc converters [5, 6, 14-17]. However, for hybrid ac-dc grids integrated with HESSs where high power and high voltage are desired, these topologies may have limitations, e.g. increased requirements of passive filters and even high step-up transformers.

Recently, the modular multilevel converter (MMC) has been widely utilized for high-voltage and high-power applications [18], [19]. In comparison with two-level converters and other multilevel converters, the salient features of the MMC include: 1) its modularity and scalability to meet high voltage level requirements, 2) reduced voltage ratings and dv/dt stress of semiconductor devices and passive components, 3) high efficiency, 4) improved power quality and reduced requirements of passive filters, 5) inherent fault-tolerance capability, and 6) fault-blocking capability to improve the post-fault performance of MMC-based applications [20]. In [21], the cost and reliability of cascaded H-bridge converters (CHBs) has been compared to two-level inverters. The conclusion is also applicable to MMCs. By increasing the number of submodules (SMs) in an MMC, the bulky and costly step-up line frequency transformer can be eliminated, which further improves system efficiency and reduces the cost and volume. Due to these attractive features, MMC is also an ideal topology for ESSs. The MMC-based battery energy storage systems

Manuscript received Oct. 25, 2017; revised Jan. 29, 2018, and April 18, 2018; accepted May 14, 2018. This work was supported by the Nanyang Technological University under Grant NTU-SUG M4081608.

Lei Zhang, **Yi Tang (corresponding author)**, and Shunfeng Yang are with the School of Electrical and Electronic Engineering, Nanyang Technological University, 50 Nanyang Avenue, 639798 Singapore. (e-mail: zhanglei19891025@gmail.com; yitang@ntu.edu.sg; syang012@e.ntu.edu.sg).

Feng Gao is with the School of Electrical Engineering, Shandong University, Jinan 250061, China. (Corresponding author. e-mail: fgao@sdu.edu.cn).

(BESSs) are proposed in [22]-[25], where batteries are distributed into each SM directly or through dc-dc converters. An MMC-based battery-SC HESS has been proposed in [26], where batteries were directly connected to the common dc-link and SCs were directly distributed into SMs. In this way, it is possible to realize decoupled power control for batteries and SCs. However, a large number of batteries should be connected in series in order to obtain a high dc-link voltage. The energy management of such a system, e.g. state of charge (SOC) balancing control of batteries may become very difficult, and additional equalizer circuits have to be employed to balance SOC as proposed in [25], which will inevitably increase the complexity of the overall system.

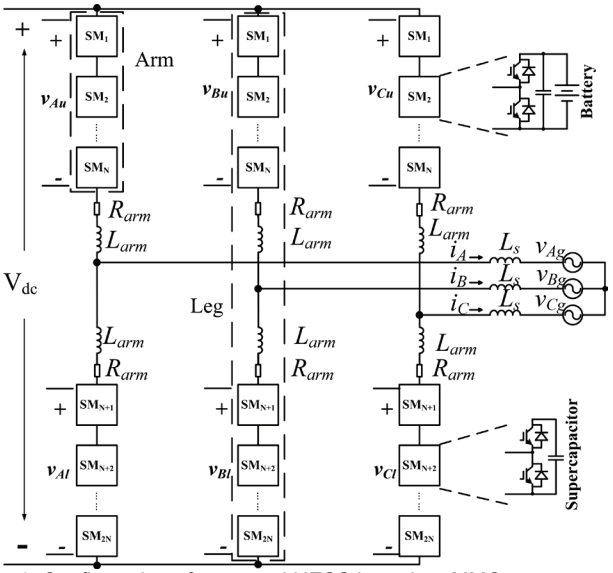

Fig. 1. Configuration of proposed HESS based on MMC.

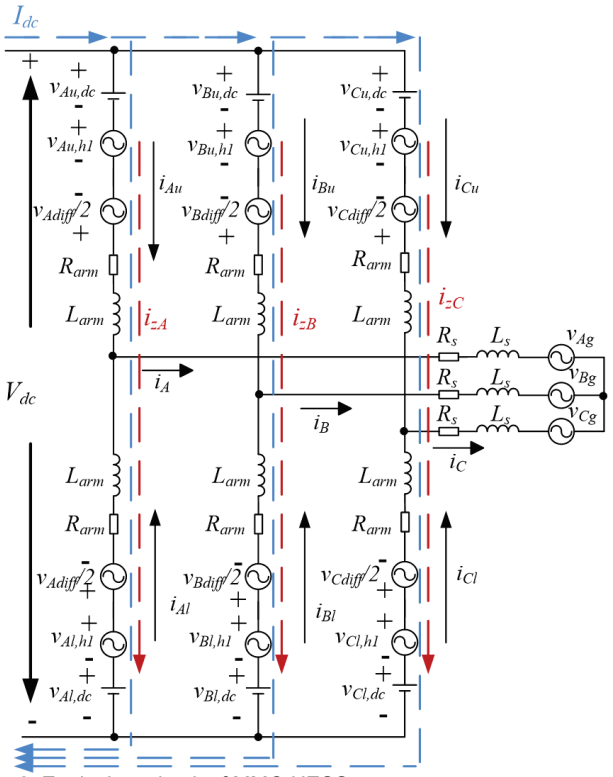

Fig. 2. Equivalent circuit of MMC-HESS.

In order to facilitate the energy management of batteries and SCs, a novel configuration of the MMC-based hybrid ac-dc grid integrated with HESS (abbreviated as MMC-HESS in this paper) is proposed in this paper and its schematic is shown in Fig. 1, where batteries and SCs are distributed into the SMs of the upper arm and the lower arm, respectively. This configuration is initially proposed in [27]. In this way, dc grid, ac grid, batteries, and SCs can be integrated into one system without employing additional semiconductor devices and passive components. Moreover, batteries and SCs are distributed into different SMs, enabling module-level power management, which will be more flexible when compared to the HESS proposed in [26].

In addition to the novel system configuration, the decoupled power control is implemented for the proposed MMC-HESS. The proposed decoupled power control can assign the power fluctuations with different timescales to batteries and SCs. Moreover, the active power and reactive power can also be decoupled and compensated by batteries and SCs respectively, which cannot be implemented by HESS based on other topologies. In this way, the power losses induced by reactive power compensation can be reduced due to the smaller equivalent series resistance (ESR) of SCs.

Finally, the operation of the proposed MMC-HESS and the mechanism of the decoupled power control will be presented in this paper and supported by laboratory experimental results. This paper will only focus on the converter-level control strategy pertaining to the proposed MMC-HESS. The system-level coordination and supervisory control of hybrid ac-dc grids are not the main focus of this paper, which have been discussed in [1]-[9].

This paper is structured as follows. Section II introduces the basic operational principle of the proposed MMC-based hybrid ac-dc grid. Section III develops a decoupled power control as well as battery SOC and SC voltage balancing strategies for the proposed system. The proposed control strategy is verified by simulation and experimental results in Section IV. Section V concludes this paper.

II. Basic Analysis of Hybrid AC-DC Grid Based on MMC

The basic operational principle of MMC has already been discussed in [18], [28] and will only be briefly reviewed here to facilitate the analysis of the control strategy presented in Section III. The SMs in each arm can be aggregated to be a single voltage source as shown in Fig. 1, i.e. the upper arm voltage v_{Xu} and the lower arm voltage v_{Xl} in phase X (X = A, B, C). Fig. 2 further reveals that the arm voltage consists of three voltage-source components. Under no load operational condition, they can also be written as,

$$\begin{cases} v_{Xu} = \dfrac{V_{dc}}{2} - v_{Xg} - \dfrac{v_{Xdiff}}{2}, \\ v_{Xl} = \dfrac{V_{dc}}{2} + v_{Xg} - \dfrac{v_{Xdiff}}{2}, \end{cases} \tag{1}$$

where V_{dc} is the dc-link voltage. The second term of each equation is mainly determined by grid voltage v_{Xg}. The second

terms of two equations have the same magnitude but are opposite in phase, and they can be utilized to regulate the active and reactive power on the ac side. v_{Xdiff} is the differential voltage.

The arm current mainly consists of three components, i.e. a dc current coming from the dc grid, a fundamental current component equals to half of the phase current, and a differential current component induced by the differential voltage, which is given by,

$$\begin{cases} i_{Xu} = \dfrac{i_{dc}}{3} + \dfrac{i_X}{2} + i_{zX} \ , \\ i_{Xl} = -\dfrac{i_{dc}}{3} + \dfrac{i_X}{2} - i_{zX} \ , \end{cases} \tag{2}$$

where i_{Xu} and i_{Xl} are the upper and lower arm currents respectively. i_X is the output phase current, and i_{zX} is the internal differential current induced by the differential voltage. Its dynamic is governed by the following equation,

$$v_{Xdiff} = 2R_{arm} i_{zX} + 2L_{arm} \frac{di_{zX}}{dt} , \tag{3}$$

where L_{arm} is the arm filter inductance and R_{arm} is the equivalent series resistance (ESR) of the filter inductor. The arm inductance can be designed according to the peak-to-peak value of the circulating current ripple. After sizing the arm inductors, the ac-side inductance can also be designed because the peak-to-peak value of the phase current ripple is determined by the sum of arm inductance and ac-side inductance [29],[30].

The discharging power of each arm can be derived from (1) and (2). Since arm and output inductors are generally very small in an MMC, their associated power can be neglected in order to simplify the analysis.

$$\begin{cases} p_{Xu} = -\dfrac{V_{dc}}{2}\left(\dfrac{i_{dc}}{3} + i_{zX,dc}\right) + v_{Xg}\left(\dfrac{i_X}{2} + i_{zX,h1}\right) + p_{Xu}^{ripple} \ , \\ p_{Xl} = -\dfrac{V_{dc}}{2}\left(\dfrac{i_{dc}}{3} + i_{zX,dc}\right) + v_{Xg}\left(\dfrac{i_X}{2} - i_{zX,h1}\right) + p_{Xl}^{ripple} \ , \end{cases} \tag{4}$$

where p_{Xu} and p_{Xl} are the instantaneous power of the upper arm and lower arm in phase X, which can be calculated from arm voltage and arm current; $i_{zX,dc}$ and $i_{zX,hl}$ are the dc component and fundamental frequency component of the internal differential current respectively.

The phase discharging power can be derived from (4), which is given by,

$$p_X = -V_{dc}\left(\frac{i_{dc}}{3} + i_{zX,dc}\right) + v_{Xg} i_X + p_X^{ripple} . \tag{5}$$

According to (4), the fundamental component of the internal differential current distributes power between the upper arm and lower arm, because the fundamental voltages of the upper arm and the lower arm are opposite in phase. For power balancing between different phase legs, it can be accomplished by tuning the internal dc differential current. As discussed in [18], [28], each phase can be regarded as a dc voltage source by neglecting all ac voltages and ac currents, and the internal dc circulating current can therefore be used to distribute power between paralleled dc voltage sources. With proper control, the internal differential current only contains dc and fundamental components. In this case, the power can be freely distributed into the two arms in the same phase by controlling the fundamental component of the internal differential current, which is also the key to realizing the decoupled power control between batteries and SCs discussed in Section III.

III. Control of Hybrid AC-DC Grid Based on MMC

The overall control system of the proposed hybrid ac-dc grid includes output power control, decoupled power control between upper arm and lower arm, SC voltage regulation, and battery SOC balancing. As mentioned in Section II, the decoupled power control is only related to the fundamental frequency component of the internal differential current, which will not affect the output power of the MMC. Therefore, the conventional output power control strategy can be adopted for the proposed hybrid ac-dc grid and will not be discussed in this paper. The SC voltage regulation and battery SOC balancing are required to maintain the proper operation of these two energy storage devices as well as MMC, and the final duty cycle of each SM can be obtained by synthesizing the outputs of all control modules. The controllers of the circulating current, average capacitor voltage, and dc-link voltage can be designed by referring to [31].

A. Decoupled power control

The instantaneous discharging power of each arm has been analyzed in Section II.

By summing the instantaneous power of three phases and transforming the fundamental frequency grid voltages and arm currents into *dq* synchronous reference frame, the total active power of the upper arm P_u and the lower arm P_l, as well as reactive power Q_u and Q_l can be derived as,

$$\begin{cases} P_u = -\dfrac{V_{dc}}{2} i_{dc} + V_g^d \underbrace{\left(\dfrac{I_g^d}{2} + I_z^d\right)}_{I_u^d} = \dfrac{P_g}{2} - \dfrac{P_{dc}}{2} + V_g^d I_z^d \ , \\ P_l = -\dfrac{V_{dc}}{2} i_{dc} + V_g^d \underbrace{\left(\dfrac{I_g^d}{2} - I_z^d\right)}_{I_l^d} = \dfrac{P_g}{2} - \dfrac{P_{dc}}{2} - V_g^d I_z^d \ . \end{cases} \tag{6}$$

$$\begin{cases} Q_u = -V_g^d I_u^q = -V_g^d \left(\dfrac{I_g^q}{2} + I_z^q\right) \ , \\ Q_l = -V_g^d I_l^q = -V_g^d \left(\dfrac{I_g^q}{2} - I_z^q\right) \ , \end{cases} \tag{7}$$

where superscripts *d* and *q* stand for the active and reactive components of voltage and current quantities respectively; I_g^d and I_g^q refer to the active and reactive components of grid current; I_z^d and I_z^q refer to the active and reactive components of internal differential current; P_g refers to the power injected into ac grid; P_{dc} refers to the power coming from dc grid. It should be noted that P_g and P_{dc} may not be equal in steady state because energy storage devices, i.e. batteries and SCs, are integrated into the SMs of the MMC.

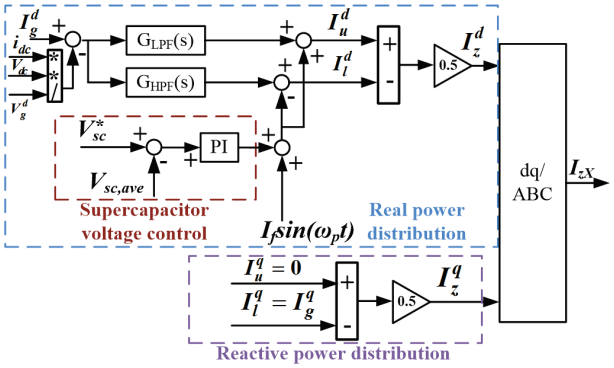

Fig. 3. Synthesis of differential current reference for decoupled power control of MMC-HESS.

From (6) and (7), the internal differential current can distribute active power and reactive power between upper arm and lower arm.

In the HESS, generally the batteries in the upper arm should compensate the long-term active power fluctuations due to their high energy capacity, and the SCs in the lower arm should cope with the short-term active power fluctuations due to their high power density. In this case, the active power compensated by batteries and SCs are related to the power difference between P_g and P_{dc}, which are given by,

$$\begin{cases} P_u = \left(P_g - P_{dc}\right) G_{LPF}(s) = \left(V_g^d I_g^d - V_{dc} i_{dc}\right) G_{LPF}(s) \\ P_l = \left(P_g - P_{dc}\right) G_{HPF}(s) = \left(V_g^d I_g^d - V_{dc} i_{dc}\right) G_{HPF}(s) \end{cases}, \tag{8}$$

where G_{LPF}(s) and G_{HPF}(s) are respectively a low pass filter (LPF) and a high pass filter (HPS) used to separate the low frequency and high frequency components in power fluctuations. The cutoff frequency of the LPF has been analyzed in references [14], [32]. In practice, this cutoff frequency should be set depending on the relative capacity of batteries and SCs. The batteries should compensate the long-term or low-frequency power fluctuations and the dc gain of the LPF is 1. In contrast, SCs should compensate transient or high-frequency power fluctuations and the dc gain of the HPF is 0.

Combining (6) and (8), the required *d*-axis component of internal differential current can be obtained as,

$$I_z^d = \left(I_g^d - \frac{V_{dc}}{V_g^d} i_{dc}\right) \frac{G_{LPF}(s) - G_{HPF}(s)}{2}. \tag{9}$$

The reactive power compensation should be solely accomplished by SCs to reduce the power losses of batteries and extend their lifespan due to the low ESR of SCs. Thus, the output reactive power of the MMC should be supplied by the lower arm,

$$\begin{cases} Q_u = 0 \\ Q_l = Q_g = -V_g^d I_g^q \end{cases}. \tag{10}$$

Similarly, combining (7) and (10) gives the *q*-axis component of differential current,

$$I_z^q = -\frac{I_g^q}{2}. \tag{11}$$

The three-phase differential current references are eventually obtained by transferring I_z^d and I_z^q back into the abc stationary reference frame. The control block diagram showing the synthesis of the internal differential current references is presented in Fig. 3. This current can be easily regulated by a proportional-integral-resonant (PIR) or more advanced repetitive controller [33], [34].

B. Battery SOC balancing control

The SOC balancing control is required to make full use of the storage capacity of batteries and also to avoid over-charging or over-discharging. The commonly used SOC estimation methods have been summarized in [35]. The SOC methods can be mainly classified as the coulomb counting method, open circuit voltage method, Kalman filter methods, impedance spectroscopy method, in which the coulomb counting method is one of the most commonly used methods. In the proposed MMC-HESS, it includes the SOC balancing between the different phases and different SMs within each arm. The SOC balancing control strategy has been proposed for the BESS based on CHB [36], [37]. For the proposed MMC-HESS, the batteries are distributed into the upper arm, which is similar to CHB. Thus, the SOC balancing control strategy proposed in [22], [36], [37] is applicable to the proposed MMC-HESS.

For analyzing the SOC balancing control, several variables are defined as follows:

$$\begin{cases} SOC_X = \dfrac{1}{N}\sum_{i=1}^{N} SOC_{Xi} \\ SOC_{ave} = \dfrac{1}{N}\left(SOC_A + SOC_B + SOC_C\right) \end{cases}, \tag{12}$$

where SOC_{Xi} is the SOC of the battery unit connected with the i^{th} SM in the upper arm of MMC; SOC_X is the average SOC of battery units in phase X (X = A, B, C) of MMC; SOC_{ave} is the average SOC of all battery units in MMC.

To balance SOCs, the discharging power of each battery unit can be individually regulated by adjusting the terminal voltage of each SM. The terminal voltage of each SM can be expressed as:

$$v_{SMi} = \frac{V_{\text{bat,Xi}}}{2}\left(1 + m\sin(\omega t) + d_{a,Xi}\right), \tag{13}$$

where $V_{bat,Xi}$ is the i^{th} battery voltage; $d_{a,Xi}$ is the additional duty ratio used to adjust the terminal voltage of SM.

To modify the terminal voltage of each SM, an additional component is added to the duty cycle of each SM, which is generated by a proportional controller, as shown in Fig. 4.

To implement the SOC balancing among three phases, the power is redistributed by a zero-sequence voltage. In this way, the ac voltages of upper arms can be expressed as:

$$\begin{bmatrix} V_{Au,ac} \\ V_{Bu,ac} \\ V_{Cu,ac} \end{bmatrix} = -\begin{bmatrix} V_{Ag} \\ V_{Bg} \\ V_{Cg} \end{bmatrix} + \begin{bmatrix} v_0 \\ v_0 \\ v_0 \end{bmatrix}. \tag{14}$$

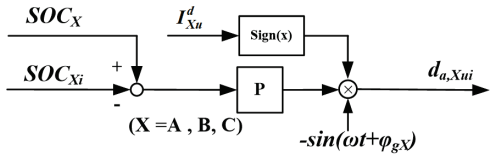

Fig. 4. SOC balancing within each arm.

The power induced by grid voltages and phase currents are still balanced. The power induced from the zero-sequence voltage can be expressed as:

$$\begin{bmatrix} P_{A0} \\ P_{B0} \\ P_{C0} \end{bmatrix} = V_0 I \begin{bmatrix} \cos(\theta_0 - \theta_I) \\ \cos(\theta_0 - \theta_I + \frac{2\pi}{3}) \\ \cos(\theta_0 - \theta_I - \frac{2\pi}{3}) \end{bmatrix}, \quad (15)$$

where θ_0 is the phase angle of zero-sequence voltage; θ_I is the phase angle of phase-A current. In this way, the power can be redistributed between the upper arms of MMC.

C. Supercapacitor voltage control

The averaged SC voltage should be maintained in an acceptable range to ensure the normal operation of MMC and enough SC energy storage capacity to compensate high-frequency power fluctuations. In order to avoid over-modulation of the lower arm, a lower limit of the averaged SC voltage should be specified based on the following equation,

$$N \cdot V_{SC,ave}^{Low} \geq 2V_{Xg,peak}, \quad (16)$$

where N is the number of SMs in the lower arm and $V_{Xg,peak}$ is the amplitude of phase voltage; $V_{SC,ave}^{Low}$ is the lower limit of the averaged SC voltage. The nominal averaged SC voltage should guarantee a sufficient storage capacity of SC. Consequently, after a transient charging or discharging process, the deviated averaged SC voltage is restored back to the nominal value. Its implementation is shown in Fig. 3. The size of SC is determined by the voltage limits and the expected discharging energy of SC [38].

In addition to the averaged SC voltage control, the voltage of SC in each SM should also be balanced to avoid SC over-voltage or under-voltage. The phase voltage balancing can be achieved by controlling the internal dc differential current. The reference of the dc internal differential current can be determined by a PI controller as depicted in Fig. 5(a). The implementation of the SC voltage balancing within each arm is shown in Fig. 5(b), which is essentially similar to that of the battery SOC balancing within each arm.

It should be noted that in steady state, the proposed inner arm SC voltage balancing method is valid only when there is a lower arm current. In the case that the dc current from dc grid is zero and there is no reactive power injected into ac grid, the lower arm current is almost zero. Under this condition, SC voltage cannot be balanced. To solve this problem, an additional low-frequency sinusoidal current reference $I_f \sin(\omega_p t)$ is added into the SC voltage control loop, as shown in Fig. 3. In this case, the SC voltage balancing control is achieved by periodically charging and discharging the SCs in the lower arm. It should be noted that the magnitude of I_f is very small and this process will stop after the voltage balancing is achieved. The associated power losses are negligible. Moreover, the angular frequency ω_p is much lower than the fundamental frequency ω and has no impact on the output regulation of MMC.

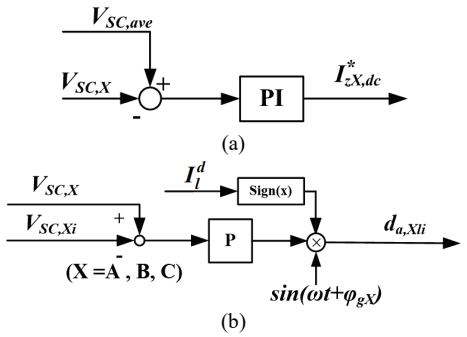

Fig. 5. SC voltage balancing control (a) between different phases, and (b) within each arm.

IV. Simulation and Experimental Results

A. Simulation results

TABLE I. Circuit Parameters of the Simulation and Experiment System

	Simulation	Experiment
Configuration	Three phase	Single phase
Grid line-line RMS voltage	10 kV	40 V
Battery unit	332 V, 5 A·h	48 V, 7 A·h
Module number per arm	64	3
Arm inductance, L_{arm}	2 mH	5 mH
AC inductance, L_s	1 mH	5 mH
DC capacitor, C	470 μF	470 μF
Supercapacitor	30,000 μF	4700 μF
DC load resistor, R_{load}	35 Ω	200 Ω
PWM carrier frequency	200 Hz	2000 Hz

The proposed MMC-HESS is simulated in Matlab/Simulink, whose configuration is the same as that shown in Fig. 1. The main parameters of the simulation model and the experimental prototype are listed in TABLE I. In experiments, the battery capacity is 7 A·h whereas it is set to be 5 A·h in simulations in order to verify the SOC balancing method within limited simulation time. The cutoff frequency of the LPF is 0.2 Hz both for simulations and experiments.

Two steady-state cases were simulated first. When P_{dc} and

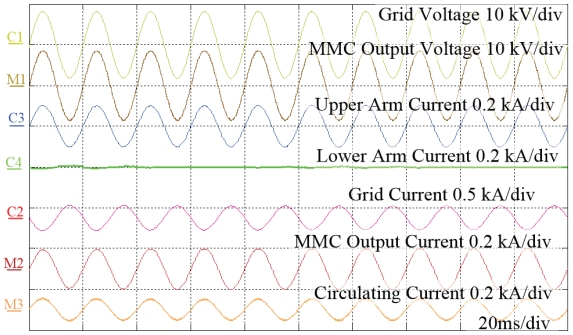

Fig. 6. Simulation results of fully compensating active power.

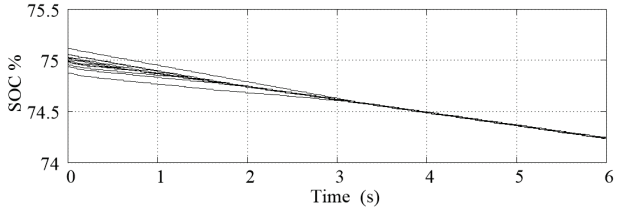

Fig. 7. Simulation results of battery SOCs balancing.

Q_g are zero, the batteries in the upper arms fully compensate the active power. The simulation results are shown in Fig. 6. When the proposed MMC-HESS reaches steady state, the upper arm current equals to the phase current of MMC, while the lower arm current almost equals to zero. During this process the battery SOCs can be balanced, as shown in Fig. 7. When P_{dc} and P_g are zero, the SCs in the lower arms should fully compensate the reactive power. The simulation results are shown in Fig. 8. As indicated in Fig. 8, the upper arm current almost equals zero, while the lower arm compensates the reactive power.

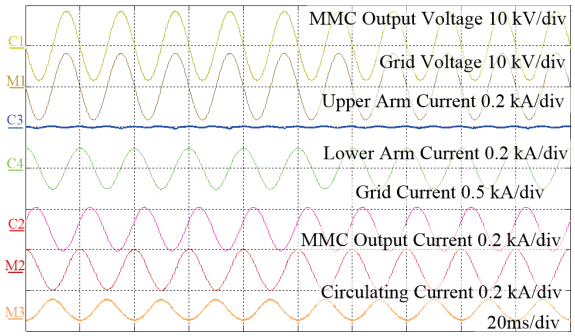

Fig. 8. Simulation results of fully compensating reactive power.

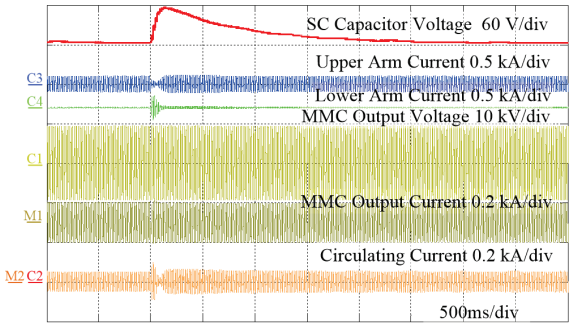

Fig. 9. Upper arm and lower arm currents, phase current, and circulating current with transition from discharging to charging of active power.

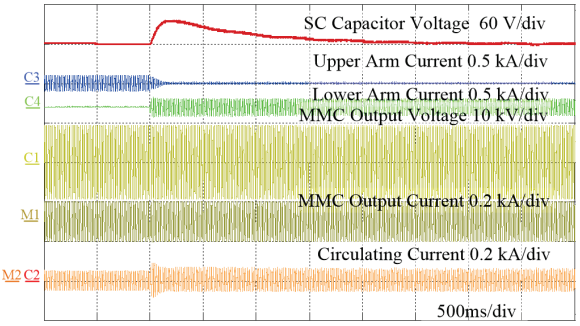

Fig. 10. Upper arm and lower arm currents, phase current, and circulating current with transition from compensating active power to reactive power.

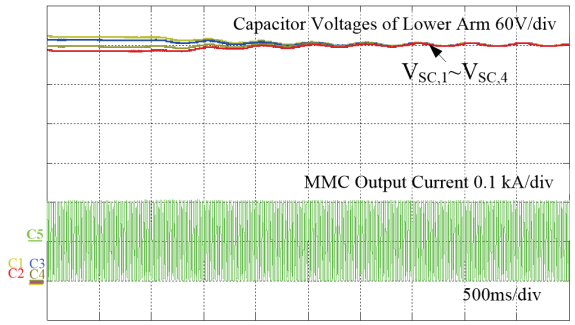

Fig. 11. Simulation results of SC voltages with P_{dc}=0, and Q_g=0.

The transition processes are also simulated. Fig. 9 indicates the transition process, when the system is switched from fully discharging to charging mode. Fig. 10 shows the transient state, when the system is switched from fully compensating active power to fully compensating reactive power.

The proposed SC voltage balancing method is verified by the simulation results, which are shown in Fig. 11. During this process, an active power is exchanged between the upper arm and lower arm periodically, which leads to a 2 Hz low-frequency voltage ripple. When the MMC-HESS reaches steady state and the SC voltages are balanced, this process can stop. Thus, as shown in Fig. 6, the arm current in steady-state does not include the 2 Hz low-frequency component as the SC voltage balancing control is disabled.

B. Experimental results

Since battery SOC balancing control has already been investigated in [22-25], the main objective of the experiments is to validate the proposed HESS and decoupled power control, and a single-phase MMC system is deemed to be sufficient. A scaled-down experimental prototype was built and tested in the laboratory, and the configuration of the experimental platform is shown in Fig. 12 with key parameters listed in TABLE I.

No load is connected to the dc-link of the MMC for better visualizing the effect of power decoupling control. In experiments, SCs were replaced by 4700 μF electrolytic capacitors to shorten the time required for SC voltage restoration and balancing control.

Fig. 13 shows the steady state experimental results of the proposed MMC-based hybrid ac-dc grid integrated with HESS. As seen, the batteries in the upper arm are put into operation when the MMC supplies active power, and the lower arm current is almost zero with only switching harmonics. Similarly, when the MMC is used for reactive power compensation, SCs will supply all reactive current to the grid, and the batteries are in the idle state with minimized power losses. These results

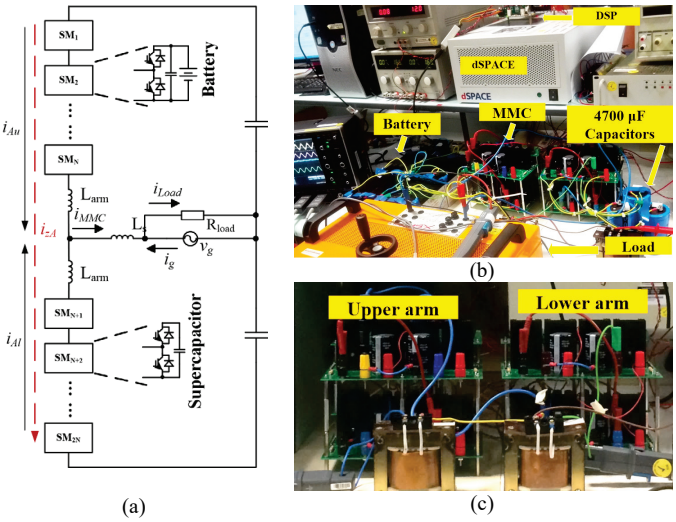

Fig. 12. Prototype (a) Schematic of experimental platform, (b) photo of laboratory prototype, and (c) sub-figure of MMC.

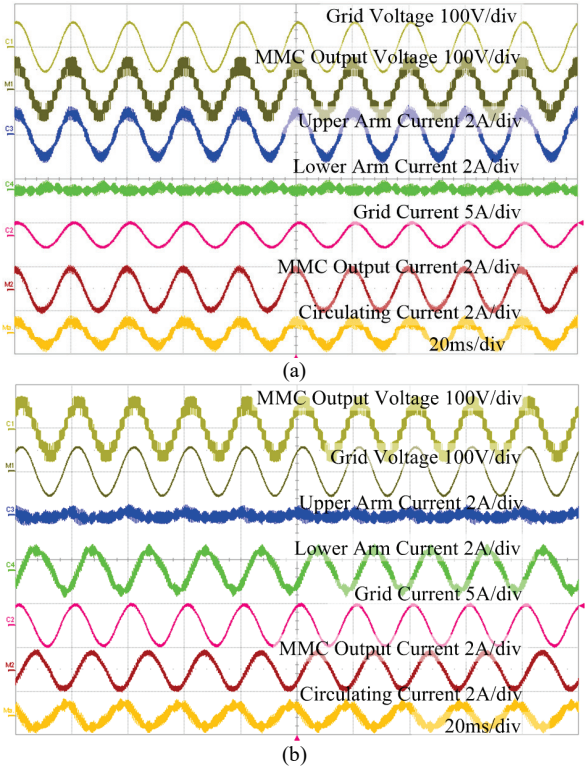

Fig. 13. Experimental results of hybrid ac-dc system with (a) active power decoupling and (b) reactive power decoupling.

successfully demonstrate the power decoupling between batteries and SCs.

Fig. 14 shows the experimental results when the proposed hybrid ac-dc grid is switched from discharging to charging mode. Since SCs are designed to cope with high frequency power fluctuations, the step change of active power is compensated by SCs to avoid over current of the batteries. In steady state, batteries with much higher energy density will replace SCs and supply active power to the grid. This proves the effectiveness of the decoupled power control governed by (8). Moreover, the SC voltage can be restored to the nominal value after the system is settled from the transient process.

Fig. 15 shows the experimental results of the proposed MMC-HESS, when it is switched from fully compensating active power to fully compensating reactive power. The SC voltage restoration control is also verified by these results, where it is clear that the SC voltages can quickly restore to the nominal value after the transient process. Fig. 16 shows the experimental results of SC voltage balancing control. As shown in Fig.16, the SC voltages can quickly converge to the nominal value after triggering the balancing control. As aforementioned, SCs basically supply zero active power in steady state and there is not enough energy to balance SC voltage within each arm. Therefore, a small low-frequency component is purposely injected to the current reference of SCs for SC voltage balancing, which will give rise to the corresponding voltage ripple in the SCs as can be observed from Fig. 16.

V. Conclusion

This paper has proposed a novel configuration of an MMC-based hybrid ac-dc grid integrated with a hybrid energy

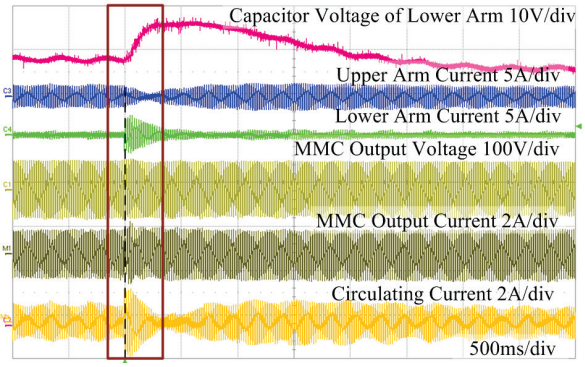

Fig. 14. Experimental results of hybrid ac-dc system with transition from discharging to charging of active power.

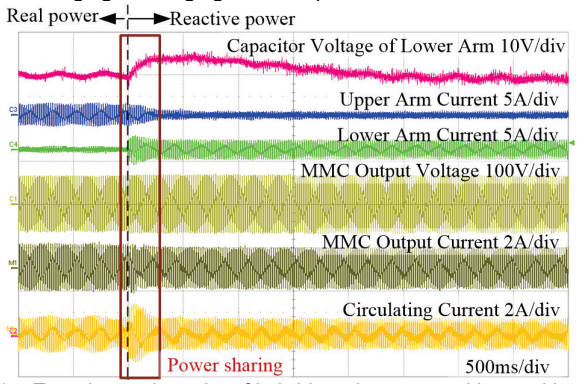

Fig. 15. Experimental results of hybrid ac-dc system with transition from compensating active power to reactive power.

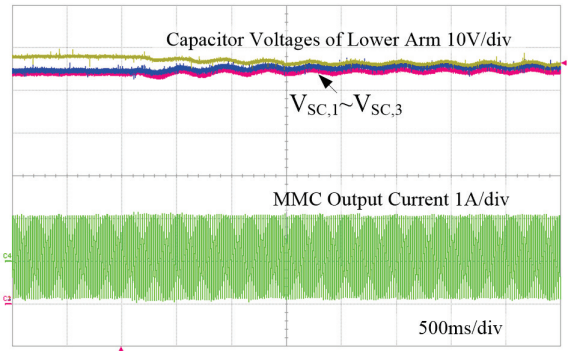

Fig. 16. Experimental results of SC voltages.

storage system, where batteries and SCs can be distributed into the upper arm and lower arm of MMC, respectively. A decoupled power control has been proposed, whose objective is to use batteries for compensation of long term active power fluctuations and SCs for compensation of short term active power fluctuations and reactive power. In this way, it is possible to simultaneously optimize the performances of batteries and SCs in the HESS by utilizing the high energy density of battery and high power density and low ESR of SC. Battery SOC balancing and SC voltage control have also been presented to improve the availability and reliability of these energy storage components. Finally, the effectiveness of the proposed MMC-based hybrid ac-dc grid and decoupled power control have been verified by simulation and laboratory experimental results.

References

[1] P.C. Loh, D. Li, Y. K. Chai, and F. Blaabjerg, "Autonomous Control of Interlinking Converter With Energy Storage in Hybrid AC–DC Microgrid," *IEEE Trans. Ind. Appl.*,vol. 49, no. 3, pp. 1374-1382, May/June. 2013.

[2] X. Liu, P. Wang, and P. C. Loh, "A Hybrid AC/DC Microgrid and Its Coordination Control," *IEEE Trans. Smart Grid,* vol. 2, pp. 278-286, 2011.

[3] X. Liu, P.C. Loh, P. Wang and F. Blaabjerg, "A Direct Power Conversion Topology for Grid Integration of Hybrid AC/DC Energy Resources," *IEEE Trans. Ind. Electron.*,vol. 60, no. 12, pp. 5696-5707, Dec. 2013.

[4] P. Wang, C. Jin, D. Zhu, Y. Tang, P. C. Loh and F. H. Choo, "Distributed Control for Autonomous Operation of a Three-Port AC/DC/DS Hybrid Microgrid," *IEEE Trans. Ind. Electron.*,vol. 62, no. 2, pp. 1279-1290, Feb. 2015.

[5] N. Eghtedarpour, and E. Farjah, "Power Control and Management in a Hybrid AC/DC Microgrid," in *IEEE Trans. Smart Grid*, vol. 5, no. 3, pp. 1494-1505, May 2014.

[6] M. Hosseinzadeh and F. R. Salmasi, "Power management of an isolated hybrid AC/DC micro-grid with fuzzy control of battery banks," in *IET Renew. Power Gen.*, vol. 9, no. 5, pp. 484-493, 7 2015.

[7] W. Kohn, Z. B. Zabinsky and A. Nerode, "A Micro-Grid Distributed Intelligent Control and Management System," in *IEEE Trans. Smart Grid*, vol. 6, no. 6, pp. 2964-2974, Nov. 2015.

[8] M. Hosseinzadeh and F. R. Salmasi, "Robust Optimal Power Management System for a Hybrid AC/DC Micro-Grid," in *IEEE Trans. Sustain. Energy*, vol. 6, no. 3, pp. 675-687, July 2015.

[9] M. Hosseinzadeh and F. Rajaei Salmasi, "Fault-Tolerant Supervisory Controller for a Hybrid AC/DC Micro-Grid," in *IEEE Trans. Smart Grid*, in press.

[10] L. Lam and P. Bauer, "Practical Capacity Fading Model for Li-Ion Battery Cells in Electric Vehicles," *IEEE Trans. Power Electron.*, vol. 28, no.12, pp. 5910-5918, Dec. 2013.

[11] A. Lahyani, P. Venet, A. Guermazi, and A. Troudi "Battery/Supercapacitors Combination in Uninterruptible Power Supply (UPS)," *IEEE Trans. Power Electron.*, vol. 28, no. 4, pp. 1509-1522, April 2013.

[12] A. Gee, F. Robinson, and R. Dunn, "Analysis of Battery Lifetime Extension in a Small-Scale Wind-Energy System Using Supercapacitors," *IEEE Trans. Energy Conversion.*, vol. 28, no. 1, pp. 24-33, March 2013.

[13] S. K. Kollimalla, M. K. Mishra and N. L. Narasamma, "Design and Analysis of Novel Control Strategy for Battery and Supercapacitor Storage System," *IEEE Trans. Sustainable Energy,* vol. 5, no. 4, pp. 1137-1144, Oct. 2014.

[14] N. R. Tummuru, M. K. Mishra and S. Srinivas, "Dynamic Energy Management of Renewable Grid Integrated Hybrid Energy Storage System," *IEEE Trans. Ind. Electron.*, vol. 62, no. 12, pp. 7728-7737, Dec. 2015.

[15] Mid-Eum Choi, Seong-Woo Kim, and Seung-Woo Seo, "Energy Management Optimization in a Battery/Supercapacitor Hybrid Energy Storage System," *IEEE Trans. Smart Grid.*, vol. 3, no. 1, pp. 463-472, March 2012.

[16] J. Cao and Ali Emadi, "A New Battery/UltraCapacitor Hybrid Energy Storage System for Electric, Hybrid, and Plug-In Hybrid Electric Vehicles," *IEEE Trans. Power Electron.*, vol. 27, no. 1, pp. 122-132, Jan. 2012.

[17] D.B. W. Abeywardana, B. Hredzak and V. G. Agelidis, "Single-Phase Grid-Connected $LiFePO_4$ Battery–Supercapacitor Hybrid Energy Storage System With Interleaved Boost Inverter," *IEEE Trans. Power Electron.*, vol. 30, no.1, pp. 5591-5604, Oct. 2015.

[18] Q. Song, W. Liu, X. Li, H. Rao, S. Xu and L. Li, "A Steady-State Analysis Method for a Modular Multilevel Converter," *IEEE Trans. Power Electron.*, vol. 28, no.8, pp. 3702-3713, Aug. 2013.

[19] M. Guan and Z. Xu, "Modeling and Control of a Modular Multilevel Converter-Based HVDC System Under Unbalanced Grid Conditions," *IEEE Trans. Power Electron.*, vol. 27, no.12, pp. 4858-4867, Dec. 2012.

[20] S. Debnath, J. Qin, B. Bahrani, M. Saeedifard and P. Barbosa, "Operation, Control, and Applications of the Modular Multilevel Converter: A Review," in *IEEE Trans. Power Electron.*, vol. 30, no. 1, pp. 37-53, Jan. 2015.

[21] Y. Xue, B. Ge and F. Z. Peng, "Reliability, efficiency, and cost comparisons of MW-scale photovoltaic inverters," 2012 IEEE Energy Conversion Congress and Exposition (ECCE), Raleigh, NC, 2012, pp. 1627-1634.

[22] M. Vasiladiotis and A. Rufer, "Analysis and Control of Modular Multilevel Converters with Integrated Battery Energy Storage," *IEEE Trans. Power Electron.*, vol. 30 no. 1, pp. 163-175, Jan. 2015.

[23] L. Zhang, F. Gao, N. Li and Q. Zhang. "Interlinking modular multilevel converter of hybrid AC-DC distribution system with integrated battery energy storage" *in Proc. 7th IEEE Energy Conversion Congress and Exposition (ECCE 2015)*, Sept. 20-24, pp. 70-77.

[24] F. Gao, L. Zhang, Q. Zhou, M. Chen and T. Xu. "State-of-Charge Balancing Control Strategy of Battery Energy Storage System Based on Modular Multilevel Converter" *in Proc. 6th IEEE Energy Conversion Congress and Exposition (ECCE 2014)*, Sept. 14-18, pp. 2567-2576.

[25] M. Quraan, T. Yeo, and P. Tricoli, "Design and Control of Modular Multilevel Converters for Battery Electric Vehicles," *IEEE Trans. Power Electron.*, vol. 31 no. 1, pp. 507-517, Jan. 2016.

[26] F. Guo and R.Sharma, " A Modular Multilevel Converter with Half-Bridge Submodules for Hybrid Energy Storage Systems Integrating Battery and UltraCapacitor," *in Proc.IEEE Appl. Power Electron. Conf. Expo(APEC2015)*, March 2015, pp. 3025-3030.

[27] L. Zhang, Yi Tang, Shunfeng Yang and F. Gao, "A modular multilevel converter-based grid-tied battery-supercapacitor hybrid energy storage system with decoupled power control," *IEEE 8th International Power Electronics and Motion Control Conference (IPEMC-ECCE Asia 2016)*, Hefei, 2016, pp. 2964-2971.

[28] K. Ilves, A. Antonopoulos, S. Norrga and H. P. Nee,"Steady-State Analysis of Interaction Between Harmonic Components of Arm and Line Quantities of Modular Multilevel Converters," *IEEE Trans. Power Electron.*, vol. 27, no. 1, pp. 57-68, Jan. 2012.

[29] Y. Li, E. A. Jones and F. Wang, "Circulating Current Suppressing Control's Impact on Arm Inductance Selection for Modular Multilevel Converter," in *IEEE J. Emerg. Sel. Topics. Power Electron.*, vol. 5, no. 1, pp. 182-188, March 2017.

[30] T. Nakanishi and J. I. Itoh, "High Power Density Design for a Modular Multilevel Converter With an H-Bridge Cell Based on a Volume Evaluation of Each Component," in *IEEE Trans. Power Electron.*, vol. 33, no. 3, pp. 1967-1984, March 2018.

[31] X. Shi, B. Liu, Z. Wang, Y. Li, L. M. Tolbert and F. Wang, "Modeling, Control Design, and Analysis of a Startup Scheme for Modular Multilevel Converters," in *IEEE Trans. Ind. Electron.*, vol. 62, no. 11, pp. 7009-7024, Nov. 2015.

[32] H. Zhou, T. Bhattacharya, D. Tran, T. S. T. Siew and A. M. Khambadkone, "Composite Energy Storage System Involving Battery and Ultracapacitor With Dynamic Energy Management in Microgrid Applications," in *IEEE Trans. Power Electron.*, vol. 26, no. 3, pp. 923-930, March 2011.

[33] Z. Li, P. Wang, Z. Chu, H. Zhu, Y. Luo and Y. Li, "An Inner Current Suppressing Method for Modular Multilevel Converters," *IEEE Trans. Power Electron.*, vol. 28, pp. 4873-4879, 2013.

[34] M. Zhang, L. Huang, W. Yao and Z. Lu, "Circulating Harmonic Current Elimination of a CPS-PWM-Based Modular Multilevel Converter With a Plug-In Repetitive Controller," *IEEE Trans. Power Electron.*, vol. 29, pp. 2083-2097, 2014.

[35] S. Piller, M. Perrin, A. Jossen, "Methods for state-of-charge determination and their applications", *J. Power Sources,* Vol. 96, No. 1, 2001, Pages 113-120.

[36] L. Maharjan, S. Inoue, H. Akagi and J. Asakura, "State-of-Charge (SOC) balancing Control of a battery energy storage system based on a Cascade PWM Converter," *IEEE Trans. Power Electron.*, vol. 24, no. 6, pp. 1628-1636, Jun. 2009.

[37] L. Maharjan, T. Yamagishi, and H. Akagi, "Active-Power Control of Individual Converter Cells for a Battery Energy Storage System Based on a Multilevel Cascade PWM Converter," *IEEE Trans. Power Electron.*, vol. 27, no. 3, pp. 1099-1107, March 2012.

[38] D. B. W. Abeywardana, B. Hredzak, V. G. Agelidis and G. D. Demetriades, "Supercapacitor Sizing Method for Energy-Controlled Filter-Based Hybrid Energy Storage Systems," in *IEEE Trans. Power Electron.* vol. 32, no. 2, pp. 1626-1637, Feb. 2017.

Lei Zhang (S'13) received the B.Eng. in electrical engineering from Shandong University of Science and Technology, Qingdao, China, in 2012. He received the M.Eng. degree in electrical engineering from Shandong University, Jinan, China, in 2015. From 2015 to 2016, he joined the School of Electrical and Electronic Engineering, Nanyang Technological University, where he worked as a Research Associate. Currently, he is working toward the Ph.D degree at the Arizona State University, Tempe, USA.
His research interests include the modular multilevel converters (MMC), energy storage system, and hybrid AC-DC microgrid.

Yi Tang (S'10-M'14-SM'18) received the B.Eng. degree in electrical engineering from Wuhan University, Wuhan, China, in 2007 and the M.Sc. and Ph.D. degrees from the School of Electrical and Electronic Engineering, Nanyang Technological University, Singapore, in 2008 and 2011, respectively.
From 2011 to 2013, he was a Senior Application Engineer with Infineon Technologies Asia Pacific, Singapore. From 2013 to 2015, he was a Postdoctoral Research Fellow with Aalborg University, Aalborg, Denmark. Since March 2015, he has been with Nanyang Technological University, Singapore as an Assistant Professor. He is the Cluster Director of the Advanced Power Electronics Research Program at the Energy Research Institute, Nanyang Technological University.
Dr. Tang was a recipient of the Infineon Top Inventor Award in 2012, the Early Career Teaching Excellence Award in 2017, and four IEEE Prize Paper Awards. He is an Associate Editor for the IEEE JOURNAL OF EMERGING AND SELECTED TOPICS IN POWER ELECTRONICS.

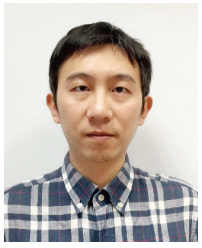

Shunfeng Yang (S'15) received the B.Eng. and M.Sc. degrees in Electrical Engineering from Southwest Jiaotong University, Chengdu, China, in 2007 and 2010, respectively. Since 2014, he has been with the School of Electrical and Electronic Engineering, Nanyang Technological University, Singapore, working towards the Ph.D. degree in power engineering.
His research interests include power electronics, multi-level converters and converter control techniques.

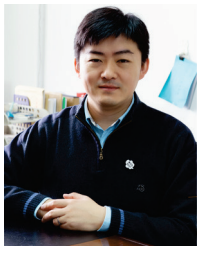

Feng Gao (S'07-M'09) received the B.Eng. and M.Eng. degrees in electrical engineering from Shandong University, Jinan, China, in 2002 and 2005, respectively, and the Ph.D. degree from the School of Electrical and Electronic Engineering, Nanyang Technological University, Singapore, in 2009. From 2008 to 2009, he was a research fellow in Nanyang Technological University. Since 2010, he joined School of Electrical Engineering, Shandong University, where he is currently a professor. From September 2006 to February 2007, he was a Visiting Scholar at the Institute of Energy Technology, Aalborg University, Aalborg, Denmark.
Dr. Gao was the recipient of the IEEE Industry Applications Society Industrial Power Converter Committee Prize for a paper published in 2006 and 2017 IEEE Power Electronics Transactions Second Prize Paper Award, and he is now serving as the Associate Editors of IEEE TRANSACTIONS ON POWER ELECTRONICS and CPSS TRANSCATIONS ON POWER ELECTRONICS AND APPLICATIONS.